

# Accurate evaluation of integrals in slender-body formulations for fibers in viscous flow

Anna-Karin Tornberg

## Abstract

A non-local slender body approximation for slender flexible fibers in Stokes flow can be derived, yielding an integral equation along the center lines of the fibers that involves a slenderness parameter. The formulation contains a so-called finite part singular integral, and can in the case of several fibers or evaluation of the flow field require the evaluation of nearly singular integrals.

We introduce a numerical technique to accurately and efficiently evaluate the finite part integral. This technique can be applied combined with any panel based quadrature rule and will add no additional cost except for a small precomputation of modified quadrature weights. We also show how a related technique that was recently introduced can be applied for the evaluation of the nearly singular integrals.

## 1 Introduction

Non-local slender body theory describes the motion of flexible fibers or filaments in viscous flows. It is based on Stokes equations, and can be used when the inertia of both fluid and fibers can be neglected, i.e. for small Reynolds numbers. Slender body theory exploits the slenderness of the fibers, and is more accurate the more slender the fiber is.

Derivations can be found in [1, 4, 3]. The result is an integral equation along the fiber center line with a slenderness parameter  $\varepsilon = r/L$ , where  $r$  is a representative radius of the fiber and  $L$  its length. Johnson [3] showed that this equation is asymptotically accurate to  $O(\varepsilon^2 \log \varepsilon)$  under some assumptions on the tapering of the fiber towards the free ends. Extending the equations to several fibers, the equations have an asymptotic accuracy of  $O(\varepsilon)$  when including both a Stokeslet and a doublet kernel (the Laplacian of the Stokeslet) [1].

Shelley and Ueda [11, 12] were the first to construct a numerical method based on a non-local slender body approximation. They did so for a closed filament (i.e. with no free ends) with its motion constrained to a plane in 3D space, studying the dynamics as the filament was set to grow everywhere along its length. Tornberg and Shelley [13] extended this work to consider multiple interacting slender fibers with free ends in a three dimensional Stokes

flow. A numerical method that included a semi-implicit treatment in time was introduced, which eliminated the severe constraint on the time step size that arise from the elasticity. Nazockdast et al. [8], further improved on this discretization, in both space and time. For a further and recent discussion on both experiments, numerical methods and the applications of flexible fibers in fluid see the recent review [10].

In this paper, we will focus on the numerical evaluation of integrals in the slender body formulation. In [13], Tornberg and Shelley introduced a regularization of the so-called finite part integral in the non-local operator to remove a solvability condition. This regularization also makes the integral non-singular, but it is still nearly singular, requiring care in its evaluation. In [13], a piecewise linear approximation of the density was assumed between grid points used to discretize the fiber such that integrals over each subinterval could be evaluated analytically. The same approach was later used in [8].

In this short note, we will focus on how to accurately evaluate the original integral, leaving the option to regularize the equations decoupled from the technique to accurately evaluate the integral. Specifically for very small values of  $\varepsilon$ , the regularization should not be needed.

We will introduce a method based on product integration to evaluate the finite part integral. This technique was introduced by Helsing and Ojala [2] to evaluate the harmonic single and double layer potentials in 2D. The technique was later extended to the Stokes equations in 2D by Ojala and Tornberg [9], and used in the simulation of viscous drops.

Another integral that appears in the slender body integral formulation contains the Stokeslet. It needs to be evaluated either to obtain the fluid velocity in the field in a post-processing step, or already in the solution step if multiple interacting fibers are considered. If the fibers get close, this integral gets nearly singular and needs special treatment for accurate evaluation. Here, we will use a method recently developed in [5], that is also an extension of the technique introduced by Helsing and Ojala [2].

After giving some preliminaries, we will discuss the special quadrature for the finite part integral in section 3, including its validation. Then we will turn to the nearly-singular Stokeslet integral. For these near-singularities a special quadrature method is developed in [5], and here we only describe and apply that method to our case.

## 2 Preliminaries

Let the centerline of a fiber be parameterized by arclength  $s \in [0, L]$ , where  $L$  is the length of the fiber, and let  $\mathbf{x}(s, t) = (x(s, t), y(s, t), z(s, t))$  describe the fiber centerline at time  $t$ . We introduce the slenderness ratio  $\varepsilon = r/L$ , where  $r$  is the radius of the fiber. Given a background velocity  $\mathbf{u}_\infty(\mathbf{x}, t) \in \mathbb{R}^3$  of the fluid with viscosity  $\mu$ , the non-local slender body approximation [1, 4, 3], gives the relation between the velocity of the fiber centerline and

the force per unit length  $\mathbf{f}(s, t) \in \mathbb{R}^3$ ,

$$8\pi\mu \left( \frac{\partial \mathbf{x}(\bar{s}, t)}{\partial t} - \mathbf{u}_\infty(\mathbf{x}(\bar{s}, t), t) \right) = -\Lambda[\mathbf{f}](\bar{s}) - \mathbf{K}[\mathbf{f}](\bar{s}), \quad \bar{s} \in [0, L]. \quad (1)$$

The local operator  $\Lambda[\mathbf{f}](\bar{s})$  is given by

$$\Lambda[\mathbf{f}](\bar{s}) = [-c(I + \hat{\mathbf{s}}\hat{\mathbf{s}}(\bar{s})) + (2 - \hat{\mathbf{s}}\hat{\mathbf{s}}(\bar{s}))]\mathbf{f}(\bar{s}), \quad (2)$$

where  $c = \log(\varepsilon^2 e)$  ( $c < 0$ ),  $\hat{\mathbf{s}}(\bar{s})$  is the unit tangent vector at  $s = \bar{s}$ , and  $\hat{\mathbf{s}}\hat{\mathbf{s}}$  is the dyadic product, i.e.  $(\hat{\mathbf{s}}\hat{\mathbf{s}})_{kl} = \hat{s}_k \hat{s}_l$ . The next term is a non-local operator, that is defined as

$$\mathbf{K}[\mathbf{f}](\bar{s}) = \int_0^L \left[ \left( \frac{I + \hat{\mathbf{R}}(s, \bar{s})\hat{\mathbf{R}}(s, \bar{s})}{|\mathbf{R}(s, \bar{s})|} \right) \mathbf{f}(s) - \left( \frac{I + \hat{\mathbf{s}}\hat{\mathbf{s}}(\bar{s})}{|s - \bar{s}|} \right) \mathbf{f}(\bar{s}) \right] ds, \quad (3)$$

where we have introduced the notation  $\mathbf{R}(s, \bar{s}) = \mathbf{x}(s) - \mathbf{x}(\bar{s})$  and  $\hat{\mathbf{R}} = \mathbf{R}/|\mathbf{R}|$ . We are here suppressing the dependence on time in the notation.

The non-local operator  $\mathbf{K}$  introduced in (3) is a so-called finite part integral. Each part is singular at  $s = \bar{s}$  and the integral is well defined only then the integrand is kept as the difference between the two terms.

The fluid velocity in a field point  $\bar{\mathbf{x}}$  can be approximated by

$$8\pi\mu (\mathbf{u}(\bar{\mathbf{x}}) - \mathbf{u}_\infty(\bar{\mathbf{x}})) = - \int_0^L \left( \frac{I}{|\mathbf{R}(s)|} + \frac{\mathbf{R}\mathbf{R}(s)}{|\mathbf{R}(s)|^3} \right) \mathbf{f}(s) ds, \quad (4)$$

where  $\mathbf{R}(s) = \bar{\mathbf{x}} - \mathbf{x}(s)$  and  $\mathbf{R}\mathbf{R}(s)$  is again a dyadic product. This kernel is the Stokeslet. Sometimes, a so-called Stokes doublet is added with an  $\varepsilon^2/2$  coefficient [1, 13].

If we consider more than one fiber, this integral will give the velocity contribution from one fiber at a point on another. In this case, (1) will be extended to a coupled system for all fibers with this interaction term [13].

This integral will be easy to resolve when  $\bar{\mathbf{x}}$  is far from the fiber, but the integrand will get increasingly peaked as  $\bar{\mathbf{x}}$  moves close to the fiber. This nearly singular case will appear e.g. when two fibers are interacting at a close distance.

## 2.1 Regular quadrature

For smooth integrals, we use a regular quadrature rule. More specifically, we will use a composite Gauss-Legendre quadrature rule, but other quadrature rules e.g. such as Clenshaw-Curtis quadrature based on Chebyshev polynomials that was used in [8] can be used.

Consider the integral of a smooth function

$$I = \int_0^L \phi(s) ds.$$

Let us now split the interval  $[0, L]$  into  $M$  intervals of equal size  $\Delta s = L/M$ , and write the integral as

$$I = \sum_{m=1}^M \int_{(m-1)\Delta s}^{m\Delta s} \phi(s) ds = \frac{\Delta s}{2} \sum_{m=1}^M \int_{-1}^1 \phi(s(\eta)) d\eta. \quad (5)$$

On each panel, we have introduced a local parameter  $\eta \in [-1, 1]$ , such that  $s_m(\eta) = (m-1)\Delta s + \frac{\Delta s}{2}(\eta+1)$  for  $s \in [m-1, m]\Delta s$ ,  $m = 1, \dots, M$ . We now introduce the Gauss-Legendre quadrature nodes  $\eta_\ell$  and weights  $w_\ell$ ,  $\ell = 1, \dots, n_{GL}$ . In this note, we will use a 16 point Gauss-Legendre rule, i.e.  $n_{GL} = 16$ , but other orders can be used. With this, we approximate

$$\int_{-1}^1 \phi(s_m(\eta)) d\eta \approx \sum_{\ell=1}^{n_{GL}} w_\ell \phi(s_m(\eta_\ell)).$$

This quadrature rule will accurately approximate the integral as long as the integrand is smooth and can be resolved with the underlying discretization.

### 3 The non-local operator

The finite part integral (3) can not be accurately evaluated using a regular quadrature method. We will start by rewriting the integral and then apply a method introduced by Helsing and Ojala [2] for a semi-analytical treatment.

#### 3.1 Rewriting the non-local operator

Let us first consider a simpler operator defined by the integral

$$\mathbb{L}[f](\bar{s}) = \int_0^L \frac{f(s) - f(\bar{s})}{|s - \bar{s}|} ds, \quad (6)$$

Rewriting this integral as

$$\mathbb{L}[f](\bar{s}) = \int_0^L g_0(s, \bar{s}) \frac{s - \bar{s}}{|s - \bar{s}|} ds, \quad (7)$$

with

$$g_0(s, \bar{s}) = \frac{f(s) - f(\bar{s})}{s - \bar{s}} \quad (8)$$

it is easy to see that

$$\lim_{s \rightarrow \bar{s}} g_0(s, \bar{s}) = f'(\bar{s}). \quad (9)$$

Similarly, we can rewrite the full  $K$  operator in (3) on this form,

$$K[\mathbf{f}](\bar{s}) = \int_0^L \mathbf{g}(s, \bar{s}) \frac{s - \bar{s}}{|s - \bar{s}|} ds, \quad (10)$$

where

$$\mathbf{g}(s, \bar{s}) = \left[ \left( I + \hat{\mathbf{R}}(s, \bar{s}) \hat{\mathbf{R}}(s, \bar{s}) \right) \frac{|s - \bar{s}|}{|\mathbf{R}(s, \bar{s})|} \mathbf{f}(s) - (I + \hat{\mathbf{s}}(\bar{s}) \hat{\mathbf{s}}(\bar{s})) \mathbf{f}(\bar{s}) \right] \frac{1}{s - \bar{s}} \quad (11)$$

The limit  $\lim_{s \rightarrow \bar{s}} \mathbf{g}(s, \bar{s})$  exists, and to find it, we first subtract and add the term  $(I + \hat{\mathbf{s}}(\bar{s}) \hat{\mathbf{s}}(\bar{s})) \mathbf{f}(\bar{s})$  inside the square bracket in (11). We then write

$$\mathbf{g}(s, \bar{s}) = \mathbf{g}_1(s, \bar{s}) + (I + \hat{\mathbf{s}}(\bar{s}) \hat{\mathbf{s}}(\bar{s})) \mathbf{g}_0(s, \bar{s}),$$

where  $\mathbf{g}_0$  is defined as  $g_0$  in (8) but with a vector valued  $\mathbf{f}(s)$ . Hence we have  $\lim_{s \rightarrow \bar{s}} \mathbf{g}_0(s, \bar{s}) = \mathbf{f}'(\bar{s})$ . There is a finite limit also for  $\mathbf{g}_1$ , and to determine the limit, we Taylor expand around  $s = \bar{s}$ . Adding the results together, we get

$$\lim_{s \rightarrow \bar{s}} \mathbf{g}(s, \bar{s}) = \frac{1}{2} (\mathbf{x}_s \mathbf{x}_{ss}(\bar{s}) + \mathbf{x}_{ss} \mathbf{x}_s(\bar{s})) \mathbf{f}(\bar{s}) + (I + \hat{\mathbf{s}} \hat{\mathbf{s}}(\bar{s})) \mathbf{f}'(\bar{s}), \quad (12)$$

where subscripts  $s$  denote derivatives with respect to arclength, and hence  $\mathbf{x}_s = \hat{\mathbf{s}}$  and  $\mathbf{x}_{ss} = \kappa \hat{\mathbf{n}}$ , where  $\kappa$  is the curvature and  $\hat{\mathbf{n}}$  the principal normal.

The operators in Eq (7) and Eq (10) are both now defined by an integral on the same form, with a smooth scalar or vector valued function multiplying the kernel  $(s - \bar{s})/|s - \bar{s}|$ . Next, we will consider how to accurately evaluate these integrals.

### 3.2 Special quadrature method

Let us now consider the evaluation of

$$I_\phi(\bar{s}) = \int_0^L \phi(s, \bar{s}) \frac{s - \bar{s}}{|s - \bar{s}|} ds. \quad (13)$$

With  $\phi = g_0$  as defined in (8), this defines the operator  $L$  in (7). If we instead let  $\phi$  denote the  $x$ ,  $y$  or  $z$  component of  $\mathbf{g}$  as defined in (11), the integral yields the corresponding component of the operator  $K$  in (10).

Dividing into subintervals as in (5), we have

$$I_\phi(\bar{s}) = \sum_{m=1}^M \int_{(m-1)\Delta s}^{m\Delta s} \phi(s, \bar{s}) \frac{s - \bar{s}}{|s - \bar{s}|} ds = \frac{\Delta s}{2} \sum_{m=1}^M \int_{-1}^1 \phi(s_m(\eta), s(\bar{\eta})) \frac{\eta - \bar{\eta}}{|\eta - \bar{\eta}|} d\eta.$$

Now, consider a panel with  $s \in [m-1, m]\Delta s$ . If the evaluation point  $\bar{s}$  lies outside of this interval,  $(s - \bar{s})/|s - \bar{s}|$  will be constant over the full interval, as there will be no shift

in sign. Since  $\phi(s, \bar{s})$  is smooth, the full integrand will be smooth over this interval, and regular quadrature can be used. For  $\bar{s} \in [m-1, m]\Delta s$ , the integrand has a discontinuity, and we will use product integration for accurate results. Let

$$\bar{\eta} = -1 + \frac{2}{\Delta s} (\bar{s} - (m-1)\Delta s),$$

s.t.  $\bar{\eta} \in [-1, 1]$ . For short, denote  $\phi_{\bar{\eta}}(\eta) = \phi(s_m(\eta), s(\bar{\eta}))$  and consider the evaluation of

$$I_m(\bar{\eta}) = \int_{-1}^1 \phi_{\bar{\eta}}(\eta) \frac{\eta - \bar{\eta}}{|\eta - \bar{\eta}|} d\eta. \quad (14)$$

Expanding  $\phi_{\bar{\eta}}(\eta)$  into a polynomial with  $n_{GL}$  terms,

$$\phi_{\bar{\eta}}(\eta) = \sum_{k=0}^{n_{GL}-1} c_k \eta^k, \eta \in [-1, 1],$$

we get

$$I_m(\bar{\eta}) = \sum_{k=0}^{n_{GL}-1} c_k \int_{-1}^1 \eta^k \frac{\eta - \bar{\eta}}{|\eta - \bar{\eta}|} d\eta = \sum_{k=0}^{n_{GL}-1} c_k q_k(\bar{\eta}), \quad (15)$$

where

$$q_k(\bar{\eta}) = \int_{-1}^1 \eta^k \frac{\eta - \bar{\eta}}{|\eta - \bar{\eta}|} d\eta = \frac{1 + (-1)^{k+1} - 2\bar{\eta}^{k+1}}{k+1}. \quad (16)$$

### 3.3 Precomputation of modified quadrature weights

We assume that we discretize the slender body integral equation using a Nyström method. This means that we collocate the equation at the quadrature nodes. Hence, on panel  $m$ , we assume that we have  $\phi$  evaluated at the Gauss-Legendre nodes  $\eta_\ell$ ,  $\ell = 1, \dots, n_{GL}$ .

We define three column vectors, *i*)  $\mathbf{p}$ , *ii*)  $\mathbf{c}$  and *iii*)  $\mathbf{q}(\bar{\eta})$ , containing the values of  $\{\phi(\eta_\ell)\}_{\ell=1}^{n_{GL}}$ ,  $\{c_k\}_{k=0}^{n_{GL}-1}$ , and  $\{q_k(\bar{\eta})\}_{k=0}^{n_{GL}-1}$ , respectively. The coefficients in  $\mathbf{c}$  are the solution to the Vandermonde system

$$A\mathbf{c} = \mathbf{p},$$

where column number  $k$  of the Vandermonde matrix  $A$  contains the values of  $\{(\eta_\ell)^{k-1}\}_{\ell=1}^{n_{GL}}$ . With this, we continue from Eq (15) and write

$$I_m(\bar{\eta}) = \mathbf{c}^T \mathbf{q}(\bar{\eta}) = (A^{-1}\mathbf{p})^T \mathbf{q}(\bar{\eta}) = \mathbf{p}^T (A^{-T} \mathbf{q}) = \mathbf{p}^T \mathbf{b}(\bar{\eta}),$$

where in the last step, we have defined the vector  $\mathbf{b}$  as the solution to

$$A^T \mathbf{b}(\bar{\eta}) = \mathbf{q}(\bar{\eta}).$$

When we solve the integral equation,  $\bar{\eta}$  will in turn take the values of all Gauss-Legendre quadrature nodes, since we collocate at these nodes. Hence, for one reference panel, we can solve  $A^T \mathbf{b}(\eta_\ell) = \mathbf{q}(\eta_\ell)$ ,  $\ell = 1, \dots, n_{GL}$ , to find the target specific weights  $\mathbf{b}(\eta_\ell)$  for each Gauss-Legendre node. Then the integral  $I_m(\eta_\ell)$  in Eq (14) can simply be evaluated using these weights,

$$I_m(\eta_\ell) = \sum_{k=1}^{n_{GL}} b_k(\eta_\ell) \phi_{\eta_\ell}(\eta_k), \quad (17)$$

where  $\phi_{\eta_\ell}(\eta_k) = \phi(s(\eta_k), s(\eta_\ell))$  as introduced above (14).

Note that only once do we need to compute the 16 target specific weights  $b_k(\eta_\ell)$  for the 16 target values  $\eta_\ell$ . They can then be used to integrate over each panel for any of the discrete target points within the panel. Remember, for evaluation points outside of the panel, regular quadrature can be used.

### 3.4 Validation and numerical tests

Götz [1] has shown that the operator  $\mathbf{L}$  in (6) diagonalizes under the Legendre polynomials  $P_n$ . Scaled to the interval  $s \in [0, L]$  this result yields

$$\mathbf{L}[\tilde{P}_n](\bar{s}) = -\lambda_n \tilde{P}_n(\bar{s}), \quad n = 0, 1, \dots \quad (18)$$

where  $\tilde{P}_n(s) = P_n(-1 + 2s/L)$  and

$$\lambda_n = \lambda_{n-1} + \frac{2}{n}, \quad n > 0 \quad \text{and} \quad \lambda_0 = 0.$$

We will start to investigate the performance of our special quadrature on this example, since there is an exact result to compare to. Note that the shape of the fiber does not enter this integration. In all our tests, we use a 16-point Gauss-Legendre rule on each panel,  $n_{GL} = 16$ .

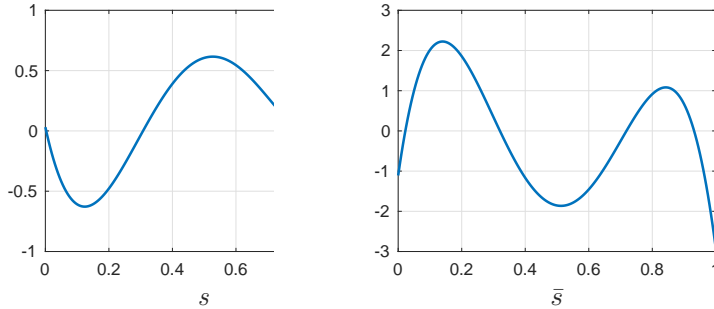


Figure 1: Left:  $f(s)$  as in (19) with  $P = 5$ . Right:  $L[f](\bar{s})$  as in (6), plotted vs  $\bar{s}$ .

In this first example, we set

$$f(s) = \sum_{n=0}^{P-1} \alpha_n \tilde{P}_n(s), \quad (19)$$

with the coefficients  $\alpha_n$  random numbers between  $-1$  and  $1$ , and we set  $L = 1$ . See figure 1 for  $f(s)$  and  $L[f](\bar{s})$ .

As expected, the errors in the results from the special quadrature are at round off level for this case, see Table 1. It does not matter here if we use 1, 2, 4 or 8 panels, since already 1 panel is sufficient to resolve this integral.

No of panels M	Maximum error special quadrature
1	$1.78 \cdot 10^{-15}$
2	$1.78 \cdot 10^{-15}$
4	$1.78 \cdot 10^{-15}$
8	$2.22 \cdot 10^{-15}$

Table 1: Error in evaluation of  $L[f](\bar{s})$  with  $f$  as in Figure 1. Error measured by comparing the values obtained using special quadrature to the diagonalization result. Maximum error taken over all  $\bar{s}_\ell$ , the  $16M$  Gauss Legendre points.

As we turn to the full operator  $K$ , we have no diagonalization result or another analytical result that we can use for validation and we opted to try the built in Matlab routine `integral` for adaptive integration. For the simpler operator  $L$ , it works well if we manually split the integration interval in two parts,  $[0, \bar{s}]$  and  $[\bar{s}, L]$ . Without this manual split of the interval, errors fluctuate by orders of magnitude for different values of  $\bar{s}$ . For  $K$ , such a split also improves the result, but the error levels are higher. With this, we can validate our results down to an error level of about  $10^{-9}$ .

Another option for validation is to compare results obtained with the special quadrature rule for different number of panels. However, the discrete Gauss-Legendre points  $\bar{s}_\ell$  do not coincide for different number of panels. In order to compare the results, we interpolate all results to a uniform grid, on each panel using the naturally defined Legendre polynomials.

Introduce a uniform grid with  $N_u = 400$  points. Compute a reference solution  $K^{Ref}(\bar{s})$  for  $K[\mathbf{f}](\bar{s})$  with 128 panels, and interpolate the result to the values of  $\bar{s}$  of this uniform grid,  $\bar{s}_\ell = \ell L/N_u$ ,  $\ell = 0, \dots, N_u$ . Now compute an approximation of  $K[\mathbf{f}](\bar{s})$  with  $M$  panels ( $K^M(\bar{s})$ ), interpolate to the uniform grid, and define

$$e_M = \max_{0 \leq \ell \leq N_u} \|K^M(\bar{s}_\ell) - K^{Ref}(\bar{s}_\ell)\|_2. \quad (20)$$

In figure 2, the results from such a convergence test is shown. Here, the fiber is set to be a helix with constant curvature and torsion, and the force is given by  $\mathbf{f}(s) =$



$(f_1(s), f_2(s), f_3(s))$ , where

$$f_1(s) = \cos(2\pi s)^2 + e^{-s} + e^{-L+s}, \quad f_2(s) = \sin(4\pi s)^2, \quad f_3(s) = e^{-2s}. \quad (21)$$

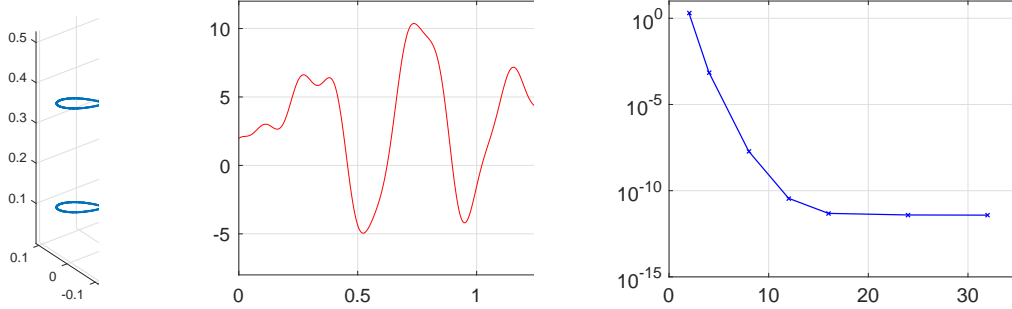


Figure 2: Left: A helix with constant curvature  $\kappa = 8$  and torsion  $\tau = 3$ , total arclength  $L = 3/2$ . Center:  $K[\mathbf{f}](\bar{s})$  plotted versus  $\bar{s}$  for  $\mathbf{f}$  in (21). Right: The error  $e_M$  (20) in approximation of  $K[\mathbf{f}](\bar{s})$  versus number of panels ( $M$ ).

however note that the error that we are measuring is not only the quadrature error, but includes also the error introduced from interpolation to the uniform grid. We believe that it is the interpolation error that makes the error curve flatten out at a level around  $10^{-12}$ .

## 4 Fluid velocity and interacting fibers

The Stokeslet integral in (4) gets very difficult to resolve as the evaluation point  $\bar{\mathbf{x}}$  gets close to the fiber, and it is not possible to deal with this difficulty simply by refinement. Doubling the number of panels, the width of the error region above a certain tolerance will approximately be halved, but the maximum error will not decrease.

### 4.1 Special quadrature method for nearly singular integral

In [5], the same underlying idea from [2] that we have already used for the finite part integral has been extended to deal with nearly singular line integrals.

Let us write the integral in (4) as

$$S[\mathbf{f}](\bar{\mathbf{x}}) = \int_0^L \left( \frac{\mathbf{f}(s)}{|\bar{\mathbf{x}} - \mathbf{x}(s)|} + \frac{((\bar{\mathbf{x}} - \mathbf{x}(s)) \cdot \mathbf{f}(s)) (\bar{\mathbf{x}} - \mathbf{x}(s))}{|\bar{\mathbf{x}} - \mathbf{x}(s)|^3} \right) ds. \quad (22)$$

Splitting the interval into panels in correspondance to (5), we write for  $p = 1, 3$

$$\int_0^L \frac{\mathbf{g}_p(s)}{|\bar{\mathbf{x}} - \mathbf{x}(s)|^p} ds = \frac{\Delta s}{2} \sum_{m=1}^M \int_{-1}^1 \frac{\mathbf{g}_p(s_m(\eta))}{|\bar{\mathbf{x}} - \mathbf{x}(s_m(\eta))|^p} d\eta,$$

with  $\mathbf{g}_p(s)$ ,  $p = 1, 3$  as understood from the two terms in (22).

Denote  $\mathbf{x}(\eta) = \mathbf{x}(s_m(\eta))$ , introduce  $R^2(\eta) = |\bar{\mathbf{x}} - \mathbf{x}(\eta)|^2$  and consider the integral

$$I_p(\bar{\mathbf{x}}) = \int_{-1}^1 \frac{g(\eta)}{(R^2(\eta))^{p/2}} d\eta = \int_{-1}^1 \tilde{g}(\eta) \frac{1}{(\omega(\eta))^{p/2}} d\eta$$

where

$$\tilde{g}(\eta) = g(\eta) \left( \frac{\omega(\eta)}{R^2(\eta)} \right)^{p/2}.$$

The idea is similar to the finite part integral, to identify an  $\omega(\eta)$  such that  $\tilde{g}(\eta)$  is regularized as compared to the original integrand, expand  $\tilde{g}(\eta)$  into a polynomial and analytically evaluate the remaining integrals.

Following [5], we define

$$\omega(\eta) = (\eta - z_1)(\eta - \bar{z}_1) = |\eta - z_1|^2,$$

where  $\{z_1, \bar{z}_1\}$  is the complex conjugate root pair of  $R^2(\eta)$  that is closest to the interval  $[-1, 1]$ . The  $q_k$ 's corresponding to (16) will then be defined as

$$q_k^p(z_1) = \int_{-1}^1 \frac{\eta^k}{\omega(\eta)^{p/2}} d\eta = \int_{-1}^1 \frac{\eta^k}{|\eta - z_1|^p} d\eta, \quad p = 1, 3.$$

Recursion formulas and a discussion about their numerical evaluation is available in [5].

Hence, the structure is the same as before, but one needs to find  $z_1$ . This is in [5] done by using a Legendre expansion of each component of  $\mathbf{x}(\eta)$  to define  $R^2(\eta)$  combined with root finding with Newton's method, see that paper for details.

Note that the special quadrature is only needed when  $\bar{\mathbf{x}}$  is close to the panel. Error estimates as derived in [6, 7] can be used to estimate the error for the regular quadrature at any  $\bar{\mathbf{x}}$  and thereby determine when to switch to special quadrature.

For the finite part integral, evaluation points are the Gauss-Legendre points on the panels. We can precompute the target specific weights for one reference panel and use them for all panels. Here, we have no prior knowledge of  $\bar{\mathbf{x}}$ , and the special quadrature weights must be computed as needed. This can however be done efficiently, see the discussion in [5].

## 4.2 Validation and numerical tests

In the numerical examples, we use the same helix as in figure 2. The helix is such that it projects onto a circle in the  $xy$ -plane. We place evaluation points inside a quarter of that circle in different  $z$ -planes, see figure 3. We evaluate  $S[\mathbf{f}](\bar{\mathbf{x}})$  (22) for all these evaluation points. We use  $\mathbf{f}(s) = (f_1(s), f_2(s), f_3(s))$ , where

$$f_1(s) = x(s) + 10 \quad f_2(s) = \sin(s), \quad f_3(s) = \cos(s), \quad (23)$$

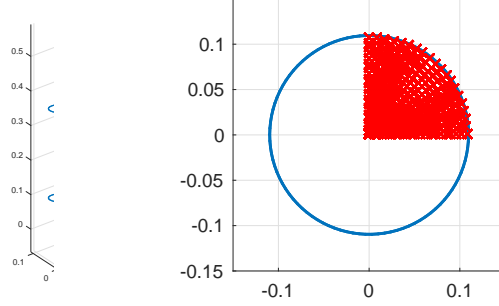


Figure 3: Left: The same helix as in figure 3, with field evaluation points.  $20 \times 20$  points are placed equidistant in polar coordinates inside the projected circle of the helix (right) with closest distance to boundary  $2.2 \cdot 10^{-3}$ . This is repeated for 16 different  $z$ -values. Right: Projection onto the  $xy$ -plane.

and also as defined in (21), which is harder to resolve. The integral (22) can be evaluated using Matlabs built in adaptive quadrature (`integral`) to high precision, and the error vector  $\mathbf{d} = (d_1, d_2, d_3)$  is defined pointwise as the difference to this reference solution. We define  $e(\bar{\mathbf{x}}) = (d_1(\bar{\mathbf{x}})^2 + d_2(\bar{\mathbf{x}})^2 + d_3(\bar{\mathbf{x}})^2)^{1/2}$  and take the maximum over all  $z$ -planes to display the errors in the  $xy$ -plane in figure 4. We take the maximum over all points to com

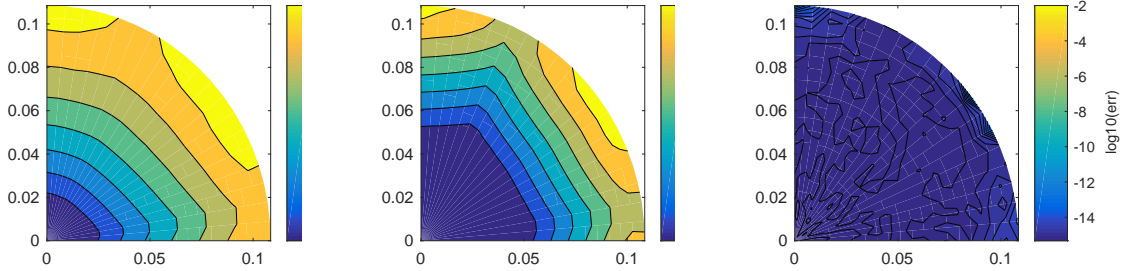


Figure 4: Error in evaluation of  $S[\mathbf{f}](\bar{\mathbf{x}})$ : Regular Gauss-Legendre quadrature with  $M = 6$  panels (left),  $M = 12$  panels (middle) and special quadrature with  $M = 8$  panels (right). The error has been taken as the maximum over all  $z$ -values for each evaluation coordinate  $(x, y)$  as in figure 3 with  $\mathbf{f}(s)$  as in (23).

pute the maximum error displayed in figure 5. From the results using regular quadrature for  $M = 6$  and  $M = 12$  panels, we can see how the error region shrinks, but how refinement fails to reduce the errors closest to the boundary. The reason that the contours are not circles is that the maximum is taken over a discrete set of  $z$ -values. The special quadrature is keeping the errors very small all the way up to the boundary. In figure 5, we can see the rapid decay of the maximum error as we increase the number of panels with which

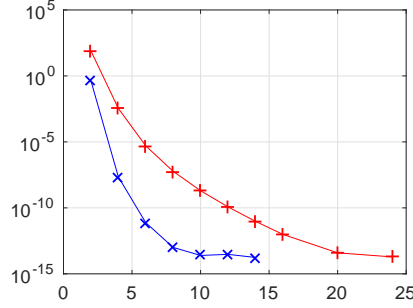


Figure 5: Maximum error in evaluation of  $S[\mathbf{f}](\bar{\mathbf{x}})$  over all the evaluation points  $\bar{\mathbf{x}}$  in figure 3 plotted versus the number of panels  $M$  for  $\mathbf{f}(s)$  as in (23) (blue line) and (21) (red line).

we discretize the helix. The special quadrature handles the singularity, but the remaining density must also be well resolved for high precision, and the figure shows the error for two different choices of  $\mathbf{f}(s)$ .

## 5 Conclusions

We have rewritten the integrand in the finite part integral as a product of two factors. The first is now smooth and we have derived an explicit formula for the limit at the problematic point. This factor is expanded as a polynomial, and the integral over each term multiplied by the second factor can be evaluated analytically. The coefficients in the polynomial expansion are defined as the solution of a Vandermonde system. We show how we can avoid to solve that system, and instead only once solve a sequence of transposed Vandermonde systems as a precomputation step, thereby defining modified quadrature weights to be used in the numerical evaluation. For a panel based quadrature with  $n$  points on each panel,  $n$  small transposed Vandermonde systems of size  $n \times n$  must be solved, and  $n^2$  target specific quadrature weights must be stored. Then the same modified quadrature weights can be used for all panels.

The singularity is hereby treated analytically and does not cause any error. The error from one panel will be determined by how well the first factor in the integrand can be approximated by an  $n - 1$  degree polynomial over that panel. In our numerical examples, we have used a 16 point Gauss-Legendre rule ( $n = n_{GL} = 16$ ).

A technique that is similar in spirit but more complicated in its detail is used for evaluation of the nearly singular integrals. Here, the evaluation point can be any point close to the fiber, and no precomputation is possible. Also in this case, we split the integrand into two factors, where the first factor is to be approximated by a polynomial such that the integral over each term can be analytically evaluated. To accomplish the split,

one however needs to find a complex conjugate pair by a root finding algorithm, and the analytical evaluation makes use of recursion formulas that require care in their numerical evaluation. This algorithm was introduced in [5]. In this paper, we have used it for the specific integrals that arise in the slender body formulation, and have shown that it does indeed yield very accurate results for evaluation points arbitrarily close to the curve.

## 6 Acknowledgements

This work is dedicated to Professor Michael Shelley on the occasion of his 60th birthday. The author wants to thank Ludvig af Klinteberg for sharing the implementation of the special quadrature method in [5]. This work was partially supported by the Göran Gustafsson Foundation for Research in Natural Sciences and Medicine, which is gratefully acknowledged.

## References

- [1] T. Götz. *Interactions of fibers and flow: Asymptotics, theory and numerics*. PhD thesis, University of Kaiserslautern, Germany, 2000.
- [2] J. Helsing and R. Ojala. On the evaluation of layer potentials close to their sources. *J. Comput. Phys.*, 227:2899–2921, 2008.
- [3] R.E. Johnson. An improved slender-body theory for Stokes flow. *J. Fluid Mech.*, 99:411–431, 1980.
- [4] J. Keller and S. Rubinow. Slender-body theory for slow viscous flow. *J. Fluid Mech.*, 75:705–714, 1976.
- [5] L. af Klinteberg and A.H. Barnett. Accurate quadrature of nearly singular line integrals in two and three dimensions by singularity swapping. *To appear*, 2019.
- [6] L. af Klinteberg and A.-K. Tornberg. Error estimation for quadrature by expansion in layer potential evaluation. *Advances in Computational Mathematics*, 43:195–234, 2017.
- [7] L. af Klinteberg and A.-K. Tornberg. Adaptive Quadrature by Expansion for layer potential evaluation in two dimensions. *SIAM J. Sci. Comput.*, 40, 2018.
- [8] E. Nazockdast, A. Rahimian, D. Zorin, and M. Shelley. Journal of Computational Physics. *J. Comput. Phys.*, 329, 2017.

- [9] R. Ojala and A.-K. Tornberg. An accurate integral equation method for simulating multi-phase Stokes flow. *J. Comput. Phys.*, 298:145–160, 2015.
- [10] O. du Roure, A. Lindner, E.N. Nazockdast, and M. J. Shelley. Dynamics of flexible fibers in viscous flows and fluids. *Annu. Rev. Fluid Mech.*, 51, 2019.
- [11] M. Shelley and T. Ueda. The nonlocal dynamics of stretching, buckling filaments. In D. Papageorgiou and Y. Renardi, editors, *Multi-Fluid Flows and Instabilities*. AMS-SIAM, 1996.
- [12] M.J. Shelley and T. Ueda. The stokesian hydrodynamics of flexing, stretching filaments. *Physica D*, 146:221–245, 2000.
- [13] A.-K. Tornberg and M.J. Shelley. Simulating the dynamics and interactions of flexible fibers in Stokes flow. *J. Comput. Phys.*, 196, 2004.